Direct Model Predictive Voltage Control of Quasi-Z-Source Inverters with *LC* Filters

Ayman Ayad, Petros Karamanakos, Ralph Kennel
Institute of Electrical Drive Systems and Power Electronics, Technische Universität München
Arcisstr. 21
80333 Munich, Germany
Phone: +49(0)89.289.28358
Fax: +49(0)89.289.28336
Email: ayman.francees@tum.de, p.karamanakos@ieee.org, ralph.kennel@tum.de
URL: http://www.eal.ei.tum.de

Keywords

≪Finite control set model predictive control≫ , ≪Z-source converter≫, ≪Voltage Source Inverters (VSI)≫ , ≪Uninterruptible Power Supply (UPS)≫ , ≪Converter control≫.

Abstract

This paper presents a direct model predictive control (MPC) strategy for the quasi-Z-source inverter connected to a linear/nonlinear load via an intermediate *LC* filter. The proposed scheme simultaneously controls the ac-side output voltage and the dc-side capacitor voltage and inductor current. The discrete-time model of the converter is derived which can be used for both modes of operations, namely the buck and boost mode. Evaluation results are presented to highlight the performance of the proposed strategy.

Introduction

The Z-source inverter (ZSI) was proposed as an alternative to the traditional voltage source inverter (VSI) [1]. Thanks to its impedance network—consisting of two identical inductors, two identical capacitors, and a diode—added to the dc side of the converter, the ZSI can operate not only in the so-called buck mode, as the VSI does, but also in the boost mode [1–3]. This is done by introducing an extra switching state (i.e. switching combination), called *shoot-through state*, that boosts the input dc voltage to the desired dc-link voltage.

To further improve the performance of the ZSI, the quasi-Z-source inverter (qZSI) was introduced [4]. This converter carries several additional advantages such as continuous input current, joint earthing of the dc source and the dc-link bus, and smaller passive components size [5] as well as increased efficiency [6, 7]. Thanks to the aforementioned advantages, the qZSI can be considered as an attractive candidate for several power electronic applications, such as photovoltaic systems, or applications where a high-quality voltage is required, e.g. energy-storage systems, distributed generations, and standalone systems.

For the latter applications, the converter is usually connected to the load via an intermediate *LC* filter to improve the quality of the output voltage. This gives rise to a higher order system, implying that the controller design becomes cumbersome when classic control methods based on linear controllers are concerned [5, 8, 9]. The reason is that such control schemes require cascaded control loops to meet the main control objective, i.e. the regulation of the output voltage to its reference value. For the qZSI, the controller design is more challenging since both the dc and ac side of the converter have to be controlled at the same time. This means that the different loops should be designed in such a way to control the dc-link voltage (i.e. the capacitor voltage) and the inductor current on the dc side of the converter as well as the filter and output variables on the ac side without interacting with each other.

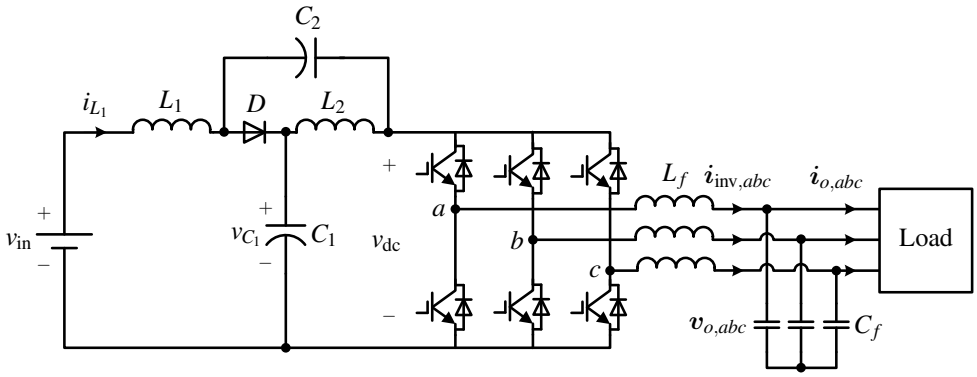

Fig. 1: The quasi-Z-source inverter (qZSI) with an *LC* filter and a load.

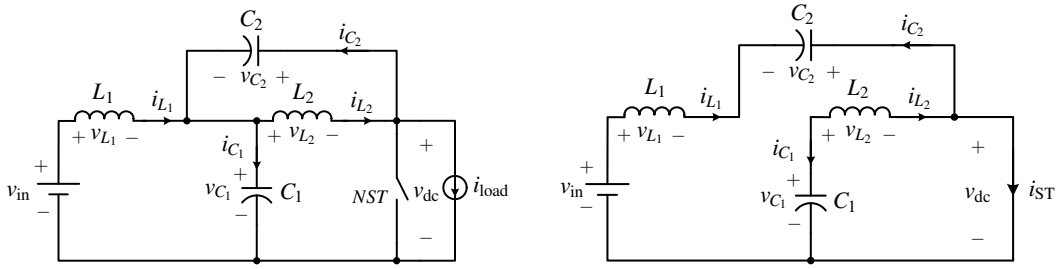

(a) Non-shoot-through state.

(b) Shoot-through state.

Fig. 2: Operation states of the qZSI during the boost mode.

A control strategy that greatly simplifies the controller design—and it is particularly suitable for multiple-input, multiple-output (MIMO) systems—is model predictive control (MPC) [10–12]. In MPC all control objectives can me tackled in one computational stage, thus multiple loops are not necessary. This is done by formulating a constrained optimization problem where a cost function that maps the objectives into a scalar is minimized. To further simplify the design of MPC schemes in power electronics, the modulation stage is included in the controller [13, 14], meaning that the algorithm directly generates the switching signals; this is the so called *direct* MPC (also referred to as finite control set (FCS) MPC) [15].

Motivated by the above-mentioned advantages of MPC, in this paper a direct MPC algorithm is implemented to control both sides of the power electronic system, consisting of a qZSI, an *LC* filter, and a linear/nonlinear load. The controller aims to directly control the output voltage without requiring a subsequent current control loop. This is in contrast to the MPC strategies introduced in the past where MPC for the qZSI was designed as a current controller, see e.g. [16–18]. However, apart from this control task, the proposed strategy should accurately regulate the capacitor voltage and the inductor current of the dc side along their reference values. To meet these goals, a discrete-time model of the system is derived that allows for the controller to accurately predict its evolution over time. Simulation and experimental results are presented to verify the effectiveness of the introduced approach.

Mathematical Model of the Quasi-Z-Source Inverter

The system under investigation, consisting of a qZSI, an *LC* filter, and a load, is shown in Fig. 1. Thanks to the inductors, L_1, L_2, and the capacitors, C_1, C_2, of the qZS network of the converter, a dc voltage v_{dc} that can be either equal to, or higher than the input voltage v_{in} can be generated. Consequently, the qZSI has two modes of operation, i.e. the buck and the boost mode; in buck mode the converter operates as the conventional two-level VSI[1], whereas in boost mode the qZSI introduces two operation states, namely the shoot-through and the non-shoot-through state, see Fig. 2.

The full model of the system can be derived by considering the different operating modes and states of

[1]In buck mode, the qZSI operates only with the non-shoot-through switching states that are used with the conventional VSI.

the qZSI. To do so, the output voltage[2] and the inverter current of the ac side as well as the inductor currents and the capacitor voltages of the dc side are chosen as state variables, i.e. the state vector is $\boldsymbol{x} = [v_{o,\alpha}\ v_{o,\beta}\ i_{\text{inv},\alpha}\ i_{\text{inv},\beta}\ i_{L_1}\ i_{L_2}\ v_{C_1}\ v_{C_2}]^T \in \mathbb{R}^8$. The three-phase switch position $\boldsymbol{u}_{abc} \in \mathcal{U}^3$, with $\boldsymbol{u}_{abc} = [u_a\ u_b\ u_c]^T$ and $\mathcal{U} = \{0,1\}$, constitutes the input vector, whereas the output voltage, along with the dc-side inductor current and capacitor voltage are the output variables, i.e. $\boldsymbol{y} = [v_{o,\alpha}\ v_{o,\beta}\ i_{L_1}\ v_{C_1}]^T \in \mathbb{R}^4$. Finally, the output current and the input voltage are considered as disturbances to the system, i.e. $\boldsymbol{w} = [i_{o,\alpha}\ i_{o,\beta}\ v_{\text{in}}]^T \in \mathbb{R}^3$.

Boost Mode Operation

As previously stated, the qZSI in boost mode operation has two types of switching states; non-shoot-through and shoot-through state. The corresponding model for each state will be separately derived as follows.

Non-Shoot-Through State

At non-shoot-through state, the diode is forward biased, thus the voltage source and the inductors deliver energy to the capacitors and the load. The system model is described by

$$\frac{\mathrm{d}\boldsymbol{x}(t)}{\mathrm{d}t} = \boldsymbol{F}_1\boldsymbol{x}(t) + \boldsymbol{G}\boldsymbol{u}_{abc}(t) + \boldsymbol{H}\boldsymbol{w}(t), \tag{1a}$$

$$\boldsymbol{y}(t) = \boldsymbol{E}\boldsymbol{x}(t), \tag{1b}$$

where [3]

$$\boldsymbol{F}_1 = \begin{bmatrix} 0 & 0 & \frac{1}{C_f} & 0 & 0 & 0 & 0 & 0 \\ 0 & 0 & 0 & \frac{1}{C_f} & 0 & 0 & 0 & 0 \\ -\frac{1}{L_f} & 0 & 0 & 0 & 0 & 0 & 0 & 0 \\ 0 & -\frac{1}{L_f} & 0 & 0 & 0 & 0 & 0 & 0 \\ 0 & 0 & 0 & 0 & 0 & 0 & -\frac{1}{L_1} & 0 \\ 0 & 0 & 0 & 0 & 0 & 0 & 0 & -\frac{1}{L_2} \\ 0 & 0 & -\frac{\boldsymbol{u}_{abc}^T\boldsymbol{K}_{(:,1)}^{-1}}{C_1} & -\frac{\boldsymbol{u}_{abc}^T\boldsymbol{K}_{(:,2)}^{-1}}{C_1} & \frac{1}{C_1} & 0 & 0 & 0 \\ 0 & 0 & -\frac{\boldsymbol{u}_{abc}^T\boldsymbol{K}_{(:,1)}^{-1}}{C_2} & -\frac{\boldsymbol{u}_{abc}^T\boldsymbol{K}_{(:,2)}^{-1}}{C_2} & 0 & \frac{1}{C_2} & 0 & 0 \end{bmatrix}$$

and

$$\boldsymbol{G} = \hat{v}_{\text{dc}} \begin{bmatrix} 0 & 0 \\ 0 & 0 \\ \frac{1}{L_f} & 0 \\ 0 & \frac{1}{L_f} \\ 0 & 0 \\ 0 & 0 \\ 0 & 0 \\ 0 & 0 \end{bmatrix} \boldsymbol{K},\ \boldsymbol{H} = \begin{bmatrix} -\frac{1}{C_f} & 0 & 0 \\ 0 & -\frac{1}{C_f} & 0 \\ 0 & 0 & 0 \\ 0 & 0 & 0 \\ 0 & 0 & \frac{1}{L_1} \\ 0 & 0 & 0 \\ 0 & 0 & 0 \\ 0 & 0 & 0 \end{bmatrix},\ \boldsymbol{E} = \begin{bmatrix} 1 & 0 & 0 & 0 & 0 & 0 & 0 & 0 \\ 0 & 1 & 0 & 0 & 0 & 0 & 0 & 0 \\ 0 & 0 & 0 & 0 & 1 & 0 & 0 & 0 \\ 0 & 0 & 0 & 0 & 0 & 0 & 1 & 0 \end{bmatrix},$$

with L_f (C_f) is the filter inductance (capacitance), and L_1, L_2 (C_1, C_2) are the inductance (capacitance) of the qZS network. Moreover, $\hat{v}_{\text{dc}}$ is the peak dc-link voltage as explained in the Appendix in [18].

Shoot-Through State

At shoot-through state, the diode does not conduct and the input voltage source and the capacitors charge the inductors. Moreover, the load is short-circuited since the upper and lower switches in at least one of

[2] To simplify the computations, it is common practice to express a variable in the stationary orthogonal system ($\alpha\beta$) instead of the three-phase system (abc), i.e. $\boldsymbol{\xi}_{\alpha\beta} = \boldsymbol{K}\boldsymbol{\xi}_{abc}$, where $\boldsymbol{K}$ is the Clarke transformation matrix of appropriate dimensions. Note, though, that, the subscript for vectors in the $\alpha\beta$ plane is dropped within the text to simplify the notation. Vectors in the *abc* plane are denoted with the corresponding subscript.

[3] For a matrix $\boldsymbol{M}$, $\boldsymbol{M}_{(:,i)}$ represents its i^{th} column.

the three phases are turned on simultaneously. Accordingly, the system model can be expressed by

$$\frac{\mathrm{d}\boldsymbol{x}(t)}{\mathrm{d}t} = \boldsymbol{F}_2\boldsymbol{x}(t) + \boldsymbol{G}\boldsymbol{u}_{abc}(t) + \boldsymbol{H}\boldsymbol{w}(t)\,, \tag{2a}$$

$$\boldsymbol{y}(t) = \boldsymbol{E}\boldsymbol{x}(t)\,, \tag{2b}$$

where

$$\boldsymbol{F}_2 = \begin{bmatrix} 0 & 0 & \frac{1}{C_f} & 0 & 0 & 0 & 0 & 0 \\ 0 & 0 & 0 & \frac{1}{C_f} & 0 & 0 & 0 & 0 \\ -\frac{1}{L_f} & 0 & 0 & 0 & 0 & 0 & 0 & 0 \\ 0 & -\frac{1}{L_f} & 0 & 0 & 0 & 0 & 0 & 0 \\ 0 & 0 & 0 & 0 & 0 & 0 & 0 & \frac{1}{L_1} \\ 0 & 0 & 0 & 0 & 0 & 0 & \frac{1}{L_2} & 0 \\ 0 & 0 & 0 & 0 & 0 & -\frac{1}{C_1} & 0 & 0 \\ 0 & 0 & 0 & 0 & -\frac{1}{C_2} & 0 & 0 & 0 \end{bmatrix}.$$

Buck Mode Operation

In buck mode, the qZSI operates as the conventional VSI. Thus, only the ac side of qZSI is considered for the system model as follows

$$\frac{\mathrm{d}\boldsymbol{x}(t)}{\mathrm{d}t} = \boldsymbol{F}_3\boldsymbol{x}(t) + \boldsymbol{G}\boldsymbol{u}_{abc}(t)\,, \tag{3a}$$

$$\boldsymbol{y}(t) = \boldsymbol{E}\boldsymbol{x}(t)\,, \tag{3b}$$

where the only nonzero entries of $\boldsymbol{F}_3$ are $\boldsymbol{F}_{3_{(1,3)}} = \boldsymbol{F}_{3_{(2,4)}} = 1/C_f$ and $\boldsymbol{F}_{3_{(3,1)}} = \boldsymbol{F}_{3_{(4,2)}} = -1/L_f$.

Continuous-Time Model

The models (1), (2) and (3) can be combined in one model which represents the different modes and states of the qZSI. First, two auxiliary binary variables d_{aux_1} and d_{aux_2} are defined. The first variable d_{aux_1} designates the state at which the converter operates in boost mode, i.e.

$$d_{\mathrm{aux}_1} = \begin{cases} 0 & \text{if non-shoot-through state} \\ 1 & \text{if shoot-through state} \end{cases}. \tag{4}$$

The second variable d_{aux_2} denotes the operation mode of the converter, i.e.

$$d_{\mathrm{aux}_2} = \begin{cases} 0 & \text{if buck mode} \\ 1 & \text{if boost mode} \end{cases}. \tag{5}$$

The transition from buck to boost mode (and vice versa) depends on whether the capacitor voltage reference ($v_{C_1,\mathrm{ref}}$) becomes greater (less) than the input dc voltage (v_{in}). When the capacitor voltage reference is higher than the input dc voltage, then the converter operates in boost mode, otherwise it works in buck mode.

Considering the defined variables in (4) and (5) with the derived models (1), (2) and (3), the full model of the converter can be expressed by

$$\frac{\mathrm{d}\boldsymbol{x}(t)}{\mathrm{d}t} = \boldsymbol{F}\boldsymbol{x}(t) + \boldsymbol{G}\boldsymbol{u}_{abc}(t) + d_{\mathrm{aux}_2}\boldsymbol{H}\boldsymbol{w}(t)\,, \tag{6a}$$

$$\boldsymbol{y}(t) = \boldsymbol{E}\boldsymbol{x}(t)\,, \tag{6b}$$

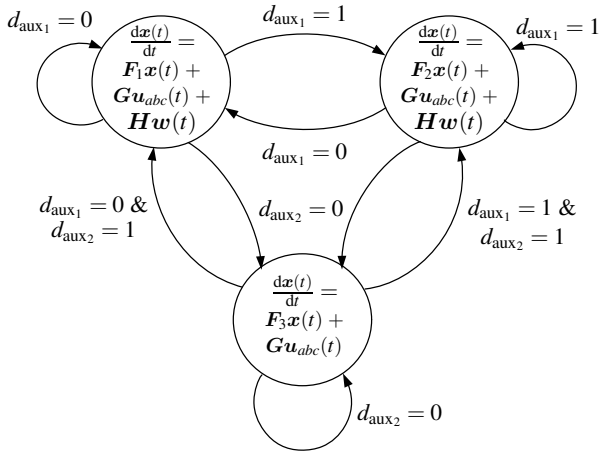

Fig. 3: The qZSI presented as a continuous-time automaton.

where $\boldsymbol{F} = \boldsymbol{F}_a + d_{\text{aux}_2}\boldsymbol{F}_b$, with $\boldsymbol{F}_a = \boldsymbol{F}_3$ and

$$\boldsymbol{F}_b = \begin{bmatrix} 0 & 0 & \frac{1}{C_f} & 0 & 0 & 0 & 0 & 0 \\ 0 & 0 & 0 & \frac{1}{C_f} & 0 & 0 & 0 & 0 \\ -\frac{1}{L_f} & 0 & 0 & 0 & 0 & 0 & 0 & 0 \\ 0 & -\frac{1}{L_f} & 0 & 0 & 0 & 0 & 0 & 0 \\ 0 & 0 & 0 & 0 & 0 & 0 & \frac{d_{\text{aux}_1}-1}{L_1} & \frac{d_{\text{aux}_1}}{L_1} \\ 0 & 0 & 0 & 0 & 0 & 0 & \frac{d_{\text{aux}_1}}{L_2} & \frac{d_{\text{aux}_1}-1}{L_2} \\ 0 & 0 & \frac{(d_{\text{aux}_1}-1)\boldsymbol{u}_{abc}^T\boldsymbol{K}_{(:,1)}^{-1}}{C_1} & \frac{(d_{\text{aux}_1}-1)\boldsymbol{u}_{abc}^T\boldsymbol{K}_{(:,2)}^{-1}}{C_1} & \frac{1-d_{\text{aux}_1}}{C_1} & -\frac{d_{\text{aux}_1}}{C_1} & 0 & 0 \\ 0 & 0 & \frac{(d_{\text{aux}_1}-1)\boldsymbol{u}_{abc}^T\boldsymbol{K}_{(:,1)}^{-1}}{C_2} & \frac{(d_{\text{aux}_1}-1)\boldsymbol{u}_{abc}^T\boldsymbol{K}_{(:,2)}^{-1}}{C_2} & -\frac{d_{\text{aux}_1}}{C_2} & \frac{1-d_{\text{aux}_1}}{C_2} & 0 & 0 \end{bmatrix}.$$

Fig. 3 shows the qZSI represented as an automaton, where the auxiliary variables d_{aux_1} and d_{aux_2} specify the transition from one condition to another.

Direct Model Predictive Voltage Control

The block diagram of the proposed direct predictive voltage controller is illustrated in Fig. 4. The proposed MPC algorithm directly sets the switch positions, thus a modulator is not needed. Based on the ac- (output voltage, inverter and output current) and dc-side (inductor current and capacitor voltage) measurements[4], the behavior of the system at the next time-step $k+1$ is computed. The switching state that results in the best future system behavior—as quantified by a performance metric—is applied to the converter.

Controller Model

Using forward Euler approximation, the continuous-time model (6) can be discretized. The resulting discrete-time model is of the form

$$\boldsymbol{x}(k+1) = \boldsymbol{A}\boldsymbol{x}(k) + \boldsymbol{B}\boldsymbol{u}_{abc}(k) + \boldsymbol{D}\boldsymbol{w}(k) \tag{7a}$$
$$\boldsymbol{y}(k) = \boldsymbol{C}\boldsymbol{x}(k), \tag{7b}$$

where $\boldsymbol{A} = (\boldsymbol{F}+\boldsymbol{I})T_s$, $\boldsymbol{B} = \boldsymbol{G}T_s$, $\boldsymbol{D} = \boldsymbol{H}T_s$ and $\boldsymbol{C} = \boldsymbol{E}$. In addition, $\boldsymbol{I}$ denotes the identity matrix, T_s is the sampling interval, and $k \in \mathbb{N}$.

[4]Note that $v_{\text{in}} = v_{C_1} - v_{C_2}$, thus it suffices to measure only the input voltage v_{in} and one capacitor voltage v_{C_1}. Moreover, only one inductor current is required to be measured since $i_{L_1} = i_{L_2}$, assuming that $L_1 = L_2$ [18].

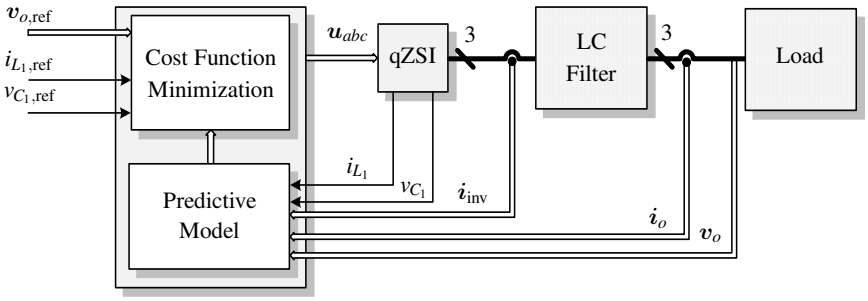

Fig. 4: Direct model predictive voltage control with reference tracking for the qZSI.

Optimization Problem

The main control objective of the proposed MPC approach is to accurately regulate the output voltage $\boldsymbol{v}_o$ along its reference value $\boldsymbol{v}_{o,\text{ref}}$ in order to keep its total harmonic distortion (THD) small. In addition, the capacitor voltage v_{C_1} and the inductor current i_{L_1} should track their reference trajectories. These objectives can be mapped into the following cost function

$$J(k) = ||\boldsymbol{y}_{\text{ref}}(k+1) - \boldsymbol{y}(k+1)||^2_{\boldsymbol{Q}} + \lambda_u ||\Delta \boldsymbol{u}_{abc}(k)||^2 . \tag{8}$$

where $\boldsymbol{y}_{\text{ref}} = [v_{o,\alpha,\text{ref}}\ v_{o,\beta,\text{ref}}\ i_{L_1,\text{ref}}\ v_{C_1,\text{ref}}]^T \in \mathbb{R}^4$. Moreover, the term $\Delta \boldsymbol{u}_{abc}(k) = \boldsymbol{u}_{abc}(k) - \boldsymbol{u}_{abc}(k-1)$ is added to control the inverter switching frequency. Finally, the weighting factor $\lambda_u > 0$ and the diagonal, positive semidefinite matrix[5] $\boldsymbol{Q} \in \mathbb{R}^{4\times 4}$ adjust the trade-off between the overall tracking accuracy and the switching frequency.

In a last step, the optimal solution $\boldsymbol{u}^*_{abc}$ is found by solving the following optimization problem

$$\begin{aligned} &\underset{\boldsymbol{u}_{abc}}{\text{minimize}} && J(k) \\ &\text{subject to} && \text{eq. (7)}. \end{aligned} \tag{9}$$

Solving (9) in real time results in the optimal switching state that is applied to the converter. Finally, at the next time-step $k+1$ the whole procedure is repeated with new measurements.

Performance Evaluation

For simulations and experiments, the system parameters are chosen as $v_{\text{in}} = 150\,\text{V}$, $L_1 = L_2 = 1\,\text{mH}$, $C_1 = C_2 = 480\,\mu\text{F}$, $L_f = 10\,\text{mH}$, $C_f = 50\,\mu\text{F}$, and the sampling time $T_s = 20\,\mu\text{s}$. The reference output voltage $v_{o,\text{ref}}$ is set to 100 V. According to [7], the capacitor voltage reference $v_{C_1,\text{ref}}$ should be more than double the output voltage reference in order not to affect the sinusoidal waveform of the output voltage. Hence, the capacitor voltage reference is chosen to be 250 V ($v_{C_1,\text{ref}} = 2.5\, v_{o,\text{ref}}$). Based on the desired output power ($P_{o,\text{ref}}$), the inductor current reference is computed by $i_{L_1,\text{ref}} = P_{o,\text{ref}}/v_{\text{in}}$. The converter operates at the targeted average switching frequency of $f_{\text{sw}} = 10\,\text{kHz}$ by setting $\boldsymbol{Q} = \text{diag}(1,1,1,0.8)$ and adjusting λ_u in the cost function (8).

Simulation Results

In this section, simulations results, based on MATLAB/Simulink, are presented that highlight the effectiveness of the proposed MPC strategy as implemented for the system under examination, see Fig. 1.

Steady-state response

The proposed controller is investigated with an *RL* linear load ($R = 10\,\Omega$, $L = 2.4\,\text{mH}$) as well as a nonlinear load in the form of a diode-bridge rectifier with a filter capacitance $C_L = 220\,\mu\text{F}$ and a resistive load $R_L = 60\,\Omega$. The simulation results of the dc and ac sides of the qZSI with the *RL* load are shown in Figs. 5 and 6, respectively. As can be observed in Fig. 5, the inductor current and the capacitor voltage

[5] The squared norm weighted with the positive (semi) definite matrix $\boldsymbol{W}$ is given by $||\boldsymbol{\xi}||^2_{\boldsymbol{W}} = \boldsymbol{\xi}^T \boldsymbol{W} \boldsymbol{\xi}$.

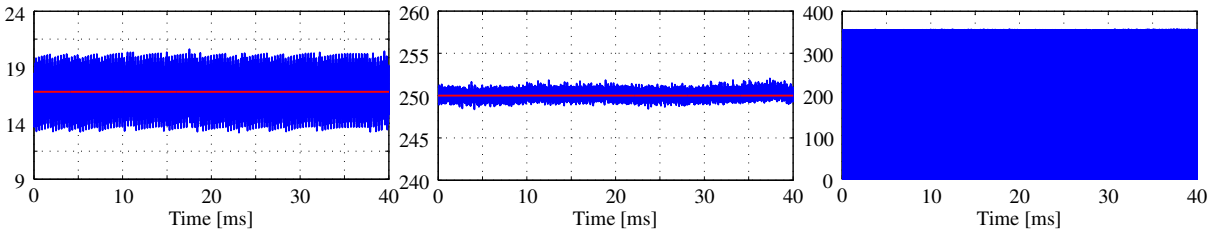

(a) Inductor current i_{L_1} and its reference in [A] (b) Capacitor voltage v_{C_1} and its reference in [V] (c) Dc-link voltage v_{dc} in [V]

Fig. 5: Simulation results of the dc side of the qZSI. $T_s = 20\mu$s, RL load $= 10\,\Omega, 2.4\,$mH, and $f_{\text{sw}} \approx 10\,$kHz.

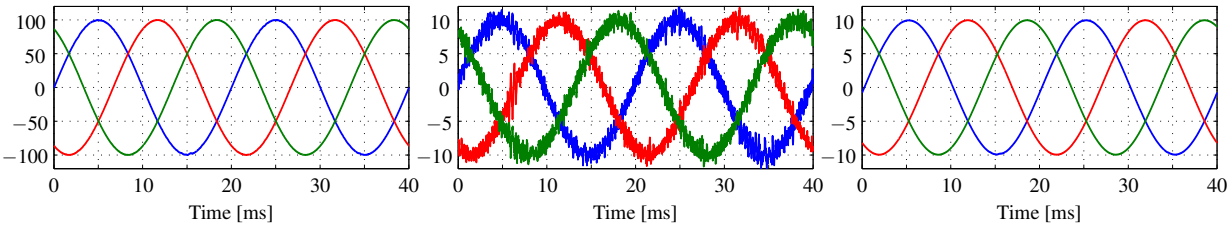

(a) Three-phase output voltage $\boldsymbol{v}_o$ in [V] (b) Three-phase inverter current $\boldsymbol{i}_{\text{inv}}$ in [A] (c) Three-phase output current $\boldsymbol{i}_o$ in [A]

Fig. 6: Simulation results of the ac side of the qZSI. $T_s = 20\mu$s, RL load $= 10\,\Omega, 2.4\,$mH, and $f_{\text{sw}} \approx 10\,$kHz. Voltage THD $= 1.15\%$.

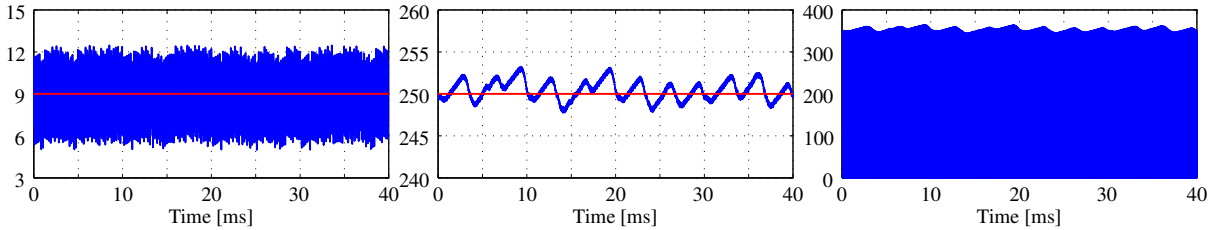

(a) Inductor current i_{L_1} and its reference in [A] (b) Capacitor voltage v_{C_1} and its reference in [V] (c) Dc-link voltage v_{dc} in [V]

Fig. 7: Simulation results of the dc side of the qZSI with a nonlinear load. $T_s = 20\mu$s and $f_{\text{sw}} \approx 10\,$kHz.

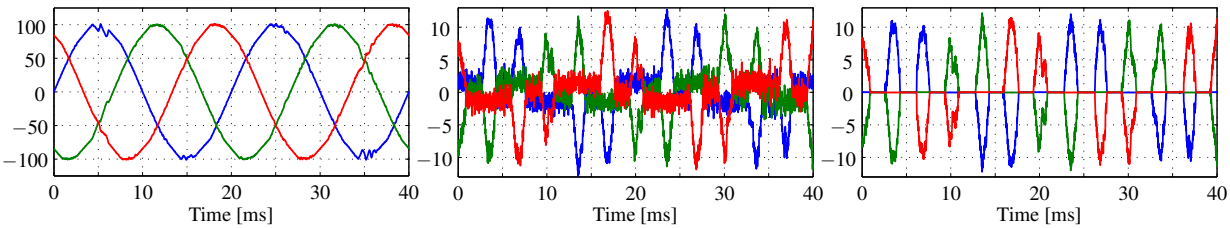

(a) Three-phase output voltage $\boldsymbol{v}_o$ in [V] (b) Three-phase inverter current $\boldsymbol{i}_{\text{inv}}$ in [A] (c) Three-phase output current $\boldsymbol{i}_o$ in [A]

Fig. 8: Simulation results of the ac side of the qZSI with a nonlinear load. $T_s = 20\mu$s and $f_{\text{sw}} \approx 10\,$kHz. Voltage THD $= 2.45\%$.

accurately track their references resulting in a boosted dc-link voltage $v_{\text{dc}} = 350\,$V. With regards to the ac side, Fig. 6 shows that the output voltage is accurately regulated along its reference with low THD (1.15%) resulting in a sinusoidal output voltage.

Moreover, the proposed MPC strategy is examined with the nonlinear load. The dc- and ac-side results are shown in Figs. 7 and 8, respectively. The inductor current and the capacitor voltage effectively track their references (Figs. 7(a) and 7(b)) resulting in a fixed boosted dc-link voltage of 350 V (Fig. 7(c)). Despite the highly distorted output current (see Fig. 8(c)) caused by the nonlinear load, the output voltage remains sinusoidal with a THD of 2.45% (see Fig. 8(a)). These results indicate that MPC is able to produce low THD output voltage not only with linear loads, but also with nonlinear loads.

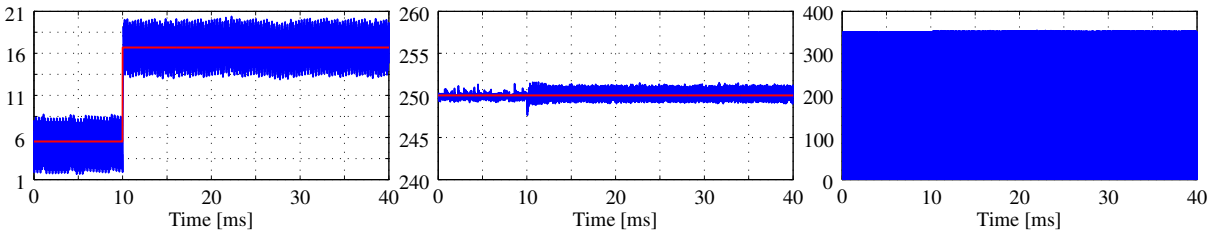

(a) Inductor current i_{L_1} and its reference in [A] (b) Capacitor voltage v_{C_1} and its reference in [V] (c) Dc-link voltage v_{dc} in [V]

Fig. 9: Simulation results of the dc side of the qZSI for a load step change from no load to full load (10 Ω, 2.4 mH). $T_s = 20\,\mu$s.

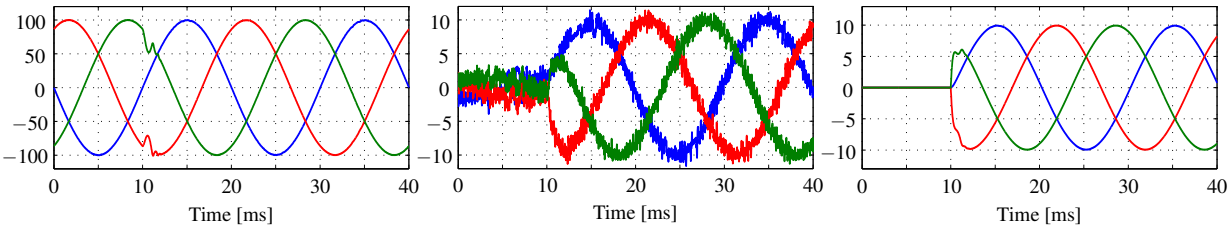

(a) Three-phase output voltage $\boldsymbol{v}_o$ in [V] (b) Three-phase inverter current $\boldsymbol{i}_{\mathrm{inv}}$ in [A] (c) Three-phase output current $\boldsymbol{i}_o$ in [A]

Fig. 10: Simulation results of the ac side of the qZSI with a load step change from no load to full load (10 Ω, 2.4 mH). $T_s = 20\,\mu$s.

Transient operation

The transient behavior of the proposed MPC strategy is examined with a resistive-inductive load. The load is step changed from no load to full load. Figs. 9 and 10 show the dc- and ac-side results, respectively. The *RL* load (10 Ω, 2.4 mH) is connected at time 10 ms. As can be seen in Fig. 9(a), the inductor current quickly tracks its reference. Moreover, the capacitor voltage is kept constant at 250 V (see Fig 9(b)) resulting in a stable dc-link voltage of 350 V (see Fig 9(c)). As for the ac side, MPC manages to quickly adjust the output voltage to its reference value as shown in Fig. 10(a). These results clearly demonstrate that MPC dynamically controls the variables of concern with very short transients.

To investigate the behavior of the MPC with both modes of operation of the qZSI, i.e. buck and boost mode, the following case is examined. The output voltage reference is changed from 50 V to 100 V, while the input voltage is kept fixed at 150 V. Accordingly, the capacitor voltage reference ($v_{C_1,\mathrm{ref}} = 2.5\,v_{o,\mathrm{ref}}$) changes from 125 V to 250 V. As stated before, the converter operates in boost mode only when the capacitor voltage reference is greater than the input dc voltage. Consequently, the qZSI works in buck mode when $v_{o,\mathrm{ref}} = 50$ V and in boost mode when $v_{o,\mathrm{ref}} = 100$ V. The dc- and ac-side results for this test are shown in Figs. 11 and 12, respectively. As can observed in Fig. 12(a), the output voltage tracks its reference both before and after the change in its reference value, i.e. both in buck and boost modes, with a very short transient time. This is thanks to the derived discrete-time model of the converter which allows for the MPC to accurately predict the system behavior not only over a limited range of operating points, but rather over the whole operating regime. On the other hand, the dc-side results show that the inductor current and the capacitor voltage quickly track their desired values, see Figs. 11(a) and 11(b), respectively.

Experimental Results

To investigate the performance of the proposed MPC strategy with the qZSI in real-time, some experiments were conducted based on an FPGA Cyclone III-EP3C40Q240C8, where preliminary results were obtained.

Figs. 13 and 14 illustrate the experimental results of the dc and ac side, respectively. Note that for the experiment, the *RL* load was changed to 20 Ω and 2.4 mH to meet the test bench requirements. As can be seen in Figs. 13(a) and 13(b) the inductor current and the capacitor voltage follow their demanded

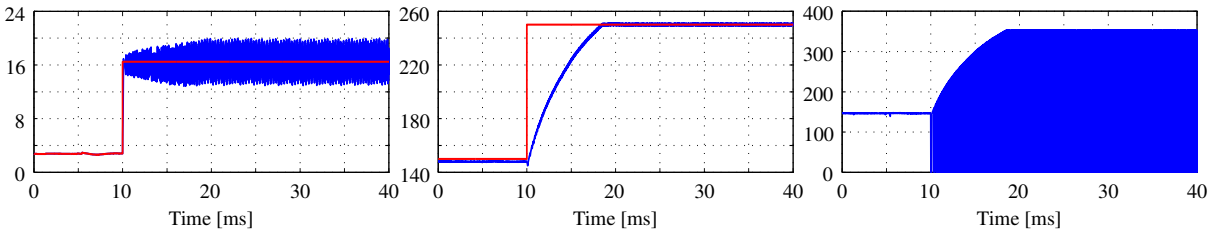

(a) Inductor current i_{L_1} and its reference in [A] (b) Capacitor voltage v_{C_1} and its reference in [V] (c) Dc-link voltage v_{dc} in [V]

Fig. 11: Simulation results of the dc side of the qZSI for a step change in the output voltage reference from 50 V to 100 V. $T_s = 20\,\mu$s.

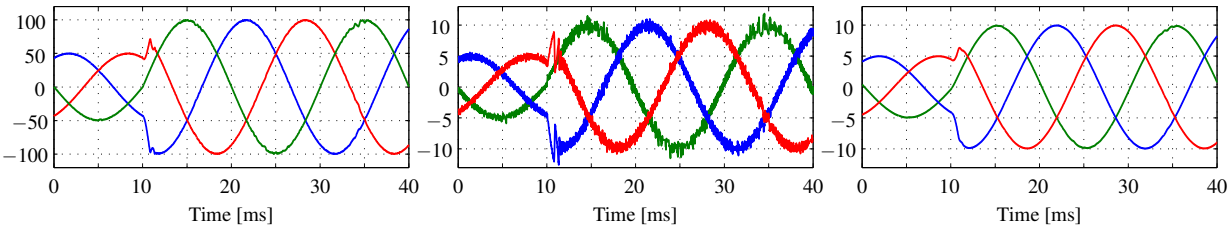

(a) Three-phase output voltage $\boldsymbol{v}_o$ in [V] (b) Three-phase inverter current $\boldsymbol{i}_{\text{inv}}$ in [A] (c) Three-phase output current $\boldsymbol{i}_o$ in [A]

Fig. 12: Simulation results of the ac side of the qZSI for a step change in the output voltage reference from 50 V to 100 V. $T_s = 20\,\mu$s.

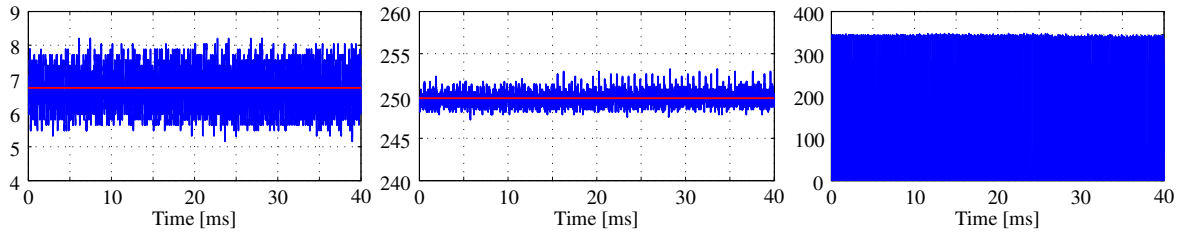

(a) Inductor current i_{L_1} and its reference in [A] (b) Capacitor voltage v_{C_1} and its reference in [V] (c) Dc-link voltage v_{dc} in [V]

Fig. 13: Experimental results of the dc side of the qZSI. $T_s = 20\,\mu$s, RL load $= 20\,\Omega$, 2.4 mH, and $f_{\text{sw}} \approx 10$ kHz.

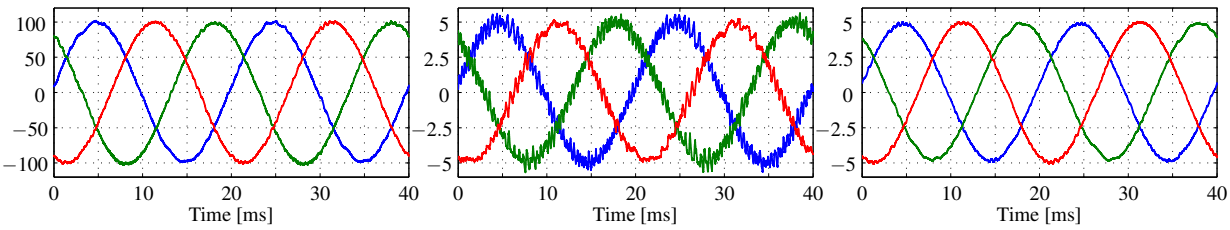

(a) Three-phase output voltage $\boldsymbol{v}_o$ in [V] (b) Three-phase inverter current $\boldsymbol{i}_{\text{inv}}$ in [A] (c) Three-phase output current $\boldsymbol{i}_o$ in [A]

Fig. 14: Experimental results of the ac side of the qZSI. $T_s = 20\,\mu$s, RL load $= 20\,\Omega$, 2.4 mH, and $f_{\text{sw}} \approx 10$ kHz. Voltage THD $= 1.29\%$.

values. Consequently, the dc-link voltage is successfully boosted to 350 V (see Fig. 13(c)). These results are in line with the simulations displayed in Fig. 5. Moreover, the output voltage reference is accurately tracked with a THD of 1.29% as shown in Fig. 14. Again, the ac-side results agree with the simulations shown in Fig. 6. These results conclude that MPC is able to control both sides of the system with a zero steady-state error for all controlled variables.

Conclusion

This paper proposes a direct model predictive voltage control for a qZSI connected to a linear/nonlinear load via an intermediate LC filter. The dc and ac side of the qZSI are simultaneously controlled in

one computational stage without requiring any subsequent control loops. More specifically, the control strategy aims to regulate the capacitor voltage and inductor current of the qZS network as well as the output voltage of the *LC* filter along their reference values. The presented results show the effectiveness of the proposed MPC strategy with both modes of operation (buck and boost mode) under both steady-state and transient operating conditions. As it is shown, MPC manages to minimize the steady-state error and features favorable behavior during transients.

References

[1] F. Z. Peng, "Z-source inverter," *IEEE Trans. Ind. Appl.*, vol. 39, no. 2, pp. 504–510, 2003.

[2] Y. Huang, M. Shen, F. Z. Peng, and J. Wang, "Z-source inverter for residential photovoltaic systems," *IEEE Trans. Power Electron.*, vol. 21, no. 6, pp. 1776–1782, Nov. 2006.

[3] A. Ayad, M. Ismeil, R. Kennel, and M. Orabi, "Experimental studies on a single-phase improved switched inductor Z-source inverter," in *Proc. Eur. Power Electron. Conf.*, Lille, France, Sep. 2013, pp. 1–10.

[4] J. Anderson and F. Peng, "Four quasi-Z-source inverters," in *Proc. IEEE Power Electron. Spec. Conf.*, Rhodes, Greece, Jun. 2008, pp. 2743–2749.

[5] Y. Li, S. Jiang, J. Cintron-Rivera, and F. Z. Peng, "Modeling and control of quasi-Z-source inverter for distributed generation applications," *IEEE Trans. Ind. Electron.*, vol. 6039, no. 4, pp. 1532–1541, Apr. 2013.

[6] A. Battiston, J. Martin, E. Miliani, B. Nahid-Mobarakeh, S. Pierfederici, and F. Meibody-Tabar, "Comparison criteria for electric traction system using Z-source/quasi-Z-source inverter and conventional architectures," *IEEE J. Emerging Sel. Top. Power Electron.*, vol. 2, no. 3, pp. 467–476, Sept. 2014.

[7] A. Ayad, S. Hanafiah, and R. Kennel, "A comparison of quasi-Z-source inverter and traditional two-stage inverter for photovoltaic application," in *Proc. Int. Expo. and Conf. Power Electron., Intelligent Motion, Renew. Energy Management*, Nuremberg , Germany, May 2015, pp. 1–8.

[8] C. J. Gajanayake, D. M. Vilathgamuwa, and P. C. Loh, "Development of a comprehensive model and a multiloop controller for Z-source inverter DO systems," *IEEE Trans. Ind. Electron.*, vol. 54, pp. 2352–2359, Aug. 2007.

[9] J. Liu, S. Jiang, D. Cao, and F. Z. Peng, "A digital current control of quasi-Z-source inverter with battery," *IEEE Trans. Ind. Informat.*, vol. 9, no. 2, pp. 928–937, May 2013.

[10] J. B. Rawlings and D. Q. Mayne, *Model Predictive Control: Theory and Design*. Madison, WI: Nob Hill, 2009.

[11] A. Linder, R. Kanchan, P. Stolze, and R. Kennel, *Model-Based Predictive Control of Electric Drives*. Cuvillier Verlag, 2010.

[12] P. Karamanakos, "Model predictive control strategies for power electronics converters and ac drives," Ph.D. dissertation, Elect. Mach. and Power Electron. Lab. NTU Athens, Athens, Greece, 2013.

[13] P. Cortés, M. P. Kazmierkowski, R. M. Kennel, D. E. Quevedo, and J. Rodríguez, "Predictive control in power electronics and drives," *IEEE Trans. Ind. Electron.*, vol. 55, no. 12, pp. 4312–4324, Dec. 2008.

[14] J. Rodríguez, M. P. Kazmierkowski, J. R. Espinoza, P. Zanchetta, H. Abu-Rub, H. A. Young, and C. A. Rojas, "State of the art of finite control set model predictive control in power electronics," *IEEE Trans. Ind. Informat.*, vol. 9, no. 2, pp. 1003–1016, May 2013.

[15] P. Karamanakos, T. Geyer, and S. Manias, "Direct voltage control of dc-dc boost converters using enumeration-based model predictive control," *IEEE Trans. Power Electron.*, vol. 29, no. 2, pp. 968–978, Feb. 2014.

[16] A. Ayad and R. Kennel, "Model predictive controller for grid-connected photovoltaic based on quasi-Z-source inverter," in *Proc. IEEE Int. Symp. Pred. Control of Elect. Drives and Power Electron.*, Munich, Germany, Oct. 2013, pp. 1–6.

[17] A. Ayad and R. Kennel, "Direct model predictive control of quasi-Z-source inverter compared with the traditional PI-based PWM control," in *Proc. Eur. Power Electron. Conf.*, Geneva, Switzerland, Sep. 2015, pp. 1–9.

[18] A. Ayad, P. Karamanakos, and R. Kennel, "Direct model predictive current control of quasi-Z-source inverters," in *Proc. IEEE Int. Symp. Pred. Control of Elect. Drives and Power Electron.*, Valparaíso, Chile, Oct. 2015, pp. 1–6.